EEG source imaging of hand movement-related areas: An evaluation of the reconstruction accuracy with optimized channels

Andres Soler[1 [0000−0002−5053−3679]], Eduardo Giraldo[2 [0000−0002−6228−2731]], and Marta Molinas[1 [0000−0002−8791−0917]]

[1] Department of Engineering Cybernetics, Norwegian University of Science and Technology, Trondheim, Norway
{andres.f.soler.guevara,marta.molinas}@ntnu.no
[2] Department of Electrical Engineering, Universidad Tecnológica de Pereira, Pereira, Colombia egiraldos@utp.edu.co

Abstract. The hand motor activity can be identified and converted into commands for controlling machines through a brain-computer-interface (BCI) system. Electroencephalography (EEG) based BCI systems employ electrodes to measure the electrical brain activity projected at the scalp and discern patterns. However, the volume conduction problem attenuates the electric potential from the brain to the scalp and introduces spatial mixing to the signals. EEG source imaging (ESI) techniques can be applied to alleviate these issues and enhance the spatial segregation of information. Despite this potential solution, the use of ESI has not been extensively applied in BCI systems, largely due to accuracy concerns over reconstruction accuracy when using low-density EEG (ldEEG), which is commonly used in BCIs. To overcome these accuracy issues in low channel counts, recent studies have proposed reducing the number of EEG channels based on optimized channel selection. This work presents an evaluation of the spatial and temporal accuracy of ESI when applying optimized channel selection towards ldEEG number of channels. For this, a simulation study of source activity related to hand movement has been performed using as starting point an EEG system with 339 channels. The results obtained after optimization show that the activity in the concerned areas can be retrieved with a spatial accuracy of 3.99, 10.69, and 14.29 mm (localization error) when using 32, 16, and 8 channel counts respectively.

Keywords: EEG, Source Imaging, Channel Optimization, Low-density EEG, BCI

1 Introduction

The human primary motor cortex (M1) has been identified as the area responsible for commanding the execution of hand movements [18]. This area is characterized for exhibiting mainly a *mu* rhythm (frequencies around 8–12 Hz) at

rest. An attenuation of the power of this rhythm, also called event-related desynchronization (ERD), in the contralateral cortex is presented during the execution/imagination of hand movements [18, 17]. This particular phenomenon in the *mu* rhythm has been exploited by brain-computer-interfaces (BCIs) to discern the hand that was executing an actual or imagined movement and convert those motor events into commands for a human peripheral system [10, 9, 19].

Most of the BCIs are based on the analysis performed using the information registered by the electrodes on the scalp (electrode space) [13], which is characterized by the low spatial resolution due to the volume conduction effect. In this, the potential generated by the electrical activity in the brain gets mixed and attenuated due to the different layers and their different conductivity properties before reaching the scalp. EEG Source imaging (ESI) methods can accurately retrieve the source activity and unmix the signals registered at the scalp; resulting in a better spatial discrimination of the underlying activity [10]. However, ESI requires high-density EEG (hdEEG) and a volume conduction model of the head, to perform accurate estimations [15]. Those requirements, in addition to computational concerns, might have contributed to fewer implementations of BCIs systems based on source activity. Despite this concern, multiple studies have demonstrated that source-centered BCIs are feasible in online scenarios [14, 2] and can outperform the electrode only based BCIs [3, 7, 23]. However, ldEEG is still preferable in BCIs due to its lower cost, increased wearability, and ease of use.

Regarding the use of ldEEG in ESI, a recent study [21], presented an automated framework for optimal selection of ldEEG electrode positions that attained higher spatial accuracy than coverage-based electrode distribution and close to hdEEG accuracy. In [12], the authors used ldEEG, 26 channels, and source space to detect lower limb movements. Although ldEEG was utilized, no optimal electrode selection was conducted and electrodes were placed based on scalp coverage criteria. Inspired by those, here we propose an evaluation of the reconstruction accuracy with optimized channels with the purpose of exploring the boundaries of ldEEG for estimating the source activity of hand movement-related areas. To perform such evaluation, first, we simulated source activity in the region of interest (ROI). Then, we applied the framework of optimal selection of electrode location from [21] and introduced new constraints to evaluate the performance of symmetrical and non-symmetrical electrode distributions. The contribution of this paper is to conduct an evaluation of how accurate can the estimation of the source activity be in the cortical hand movement-related areas, and provide information that can facilitate closing the gap between ESI and BCIs.

2 Simulation of source activity in the hand movement-related areas

To simulate activity we made use of the EEG forward equation that defines the EEG:

$$\boldsymbol{y} = \boldsymbol{M}\boldsymbol{x} + \varepsilon \tag{1}$$

In it, the matrix $\boldsymbol{y}$ represents the EEG channel data. The matrix $\boldsymbol{x}$ represents the time courses of the source activity. The matrix $\boldsymbol{M}$, often called the lead field matrix, represents the morphology and conductivity of the brain and contains the linear relationship between the cortical sources and the signals at the scalp. The matrix ε represents the noise registered in the measurements. We followed these steps for the simulations: forward modeling, ROI definition, simulation of source time courses, EEG computation, and noise addition.

Forward Modeling: To obtain the lead field matrix $\boldsymbol{M}$, we computed a boundary element method (BEM) model based on the MRI images of a 27-year-old subject. The MRI images were processed and segmented using Freesurfer [4], and the BEM surfaces of the scalp, skull, and brain were generated using Freesurfer and MNE-python [8]. A set of 339 electrodes named and positioned according to the international 10-05 system were co-registered and projected into the scalp. Then, the lead field matrix for the 10-05 set was computed using the BEM surfaces and the projected electrodes. The number of sources was defined as 4098 per hemisphere, and the default MNE-python conductivities of 0.3, 0.006 , and 0.3 S/m were used for scalp, skull, and brain, respectively.

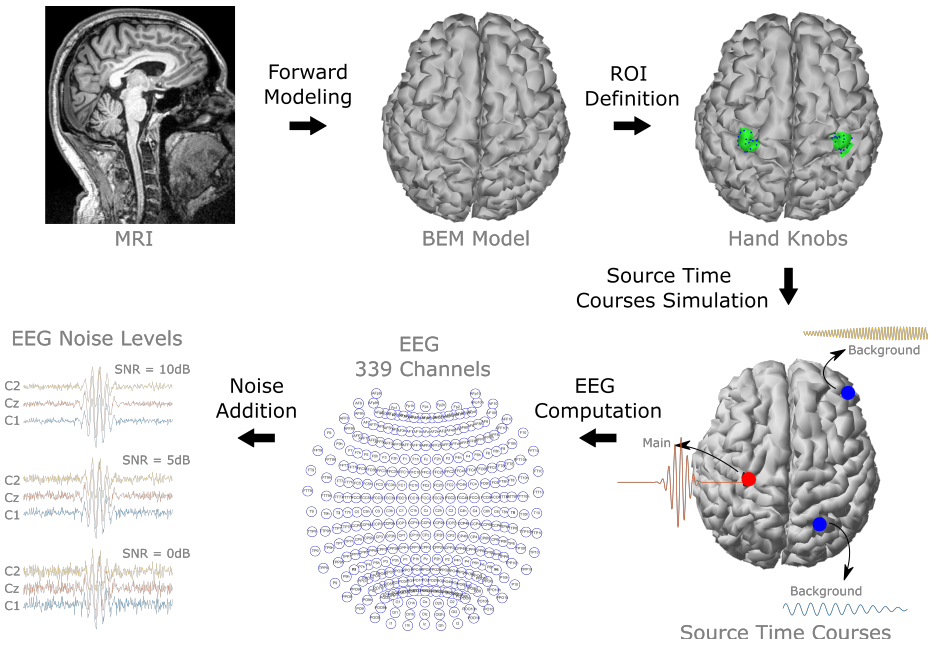

Fig. 1. Simulation procedure of the source activity in the hand movement-related areas.

ROI Definition: Previous studies [1, 3, 24, 10] have identified the sensory-motor cortex as the source regions where the upper limp movements take place, in particular, the so-called *hand knob* of the precentral gyrus has been found common across these studies. To define the ROI in the hand knobs we inspected the 3D surface of the cortex and manually labeled the center of the hand knob in each hemisphere. Two sets of sources around the markers were established by selecting the 20 closest sources to each marker. The 40 source locations and hand knobs ROIs are depicted in figure 1.

Simulation of source time-courses: Two epochs of 2 s were simulated per each source in the ROIs, resulting in 80 epochs. In each epoch three sources were activated: the main source within the ROIs and two more background sources outside them. The sources were generated using a sinusoidal Gaussian windowed activity as in [22, 21], by using the following equation:

$$x_i(t) = a_i e^{-\frac{1}{2}(\frac{t-c_i}{\sigma})^2} sin(2\pi f_i t) \tag{2}$$

The time course of the $i-th$ source is defined by the maximum amplitude a_i, the time center c_i, frequency f_i, and window width σ_i. The three activities were centered at 1 s. The main source was simulated with a frequency of 10 Hz and width 0.12. The background sources were simulated outside the ROIs to emulate brain activity from other areas and generate interference to the ESI algorithms, their location was randomly selected and they should be at least 3 cm from the main source. Their amplitude was 10 % of the amplitude of the main source, with a width of 0.12 and frequencies of 5 and 20 Hz.

EEG computation and noise addition: The EEG was computed using the forward equation 1, and the matrices $\boldsymbol{M}$ and $\boldsymbol{x}$ generated at forward modeling and source time courses simulation stages. After obtaining the matrix $\boldsymbol{y}$, Gaussian noise was added to represent the noise in the measurements, three different levels of signal-to-noise ratio were used 10, 5, and 0 dB.

Figure 1 summarizes the procedure of simulation of source activity in the hand movement-related areas.

3 Optimal selection of EEG Channels

To select and reduce the number of channels, we used the automatic methodology for electrode selection presented in [21]. In it, the non-dominated sorting genetic algorithm II (NSGA-II) is combined with ESI algorithms. The number of channels used during ESI and the localization error are minimized in a multi-objective optimization problem. In the genetic algorithm each channel position is represented by a binary value, and the set of channels by a binary vector, when the binary value corresponding to a channel is one, the channel is used during ESI, otherwise the channel is not used and its information is zeroing. The NSGA-II generates and tests multiple channel combinations while evolving them to find the ones with lower channel counts and the lower localization error.

Algorithm modification: In the original work, authors applied the methodology over epochs, therefore combinations of channels were optimized in each

epoch. In this work, we introduced a main modification: the optimization is performed over all epochs to obtain a single combination instead of an epoch-wise combination.

Constraints: We performed multiple tests in an attempt to identify combinations that leads to the lower reconstruction errors: constraining the search space to the 10-10 standard electrode placement, without search space constraint, adding a symmetricity constraint to maintain the number of channels equal between both hemispheres and performed cascade search optimization. In the cascade search, we performed three nested optimizations for 32, 16, and 8 channels, the second and third optimization were constrained to the previous combination found.

ESI algorithms: The standardized low-resolution electromagnetic tomography (sLORETA) [16] and weighted minimum norm estimation (wMNE) [6] were used to estimate the source activity during NSGA-II optimization. These algorithms were selected based on the results of previous work in [20, 21], where multiple ESI algorithms were evaluated in ldEEG conditions, and it was found that wMNE and sLORETA consistently obtained the lowest source localization errors. Both algorithms are based on minimum norm estimation, where the ESI problem can be considered as an optimization problem as follows:

$$\boldsymbol{J} = argmin_{(\boldsymbol{x})}\{||\boldsymbol{M}\boldsymbol{x} - \boldsymbol{y}||_2^2\} \tag{3}$$

As the number variables to estimate (source activity $\boldsymbol{x}$) is much higher that the number of observations (EEG channels $\boldsymbol{y}$) the problem is mathematically ill-posed and ill-conditioned [11]. This means that infinite solutions for the source activity $\boldsymbol{x}$ can be found to minimize $\boldsymbol{J}$ and fit with the EEG data $\boldsymbol{y}$. To find a unique solution, the algorithms make use of Tikhonov-Phillips regularization by including a regularization parameter λ that weights the norm of the estimated solution:

$$\boldsymbol{J} = argmin_{(\boldsymbol{x},\lambda)}\{||\boldsymbol{M}\boldsymbol{x} - \boldsymbol{y}||_2^2 + \lambda^2||\boldsymbol{x}||_2^2\} \tag{4}$$

The ESI solutions of wMNE and sLORETA are given by the following equations:

$$\hat{\boldsymbol{x}}_{wMNE} = \boldsymbol{W}^{-1}\boldsymbol{M}^T(\boldsymbol{M}\boldsymbol{W}^{-1}\boldsymbol{M}^T + \lambda^2 I)^{-1}\boldsymbol{y} \tag{5}$$

$$\hat{\boldsymbol{x}}_{sLOR} = \sqrt{\frac{1}{[\boldsymbol{S}_x]_{ii}}}\boldsymbol{M}^T(\boldsymbol{M}\boldsymbol{M}^T + \lambda^2 I)^{-1}\boldsymbol{y} \tag{6}$$

The solution of wMNE uses a weighting matrix $\boldsymbol{W}$ to influence the weight of the deep sources, resulting in a better localization of the source activity of the deeper sources [5]. Its value is computed using the following equation:

$$\boldsymbol{W}^{-1} = diag\left[\frac{1}{\|l_1\|_2}, \frac{1}{\|l_2\|_2}, ..., \frac{1}{\|l_s\|_2}\right] \tag{7}$$

where $\boldsymbol{W}$ is a diagonal matrix, and $\|l_s\|_2$ the Euclidean norm of the s-th column of $\boldsymbol{M}$

The solution of sLORETA is usually smooth (estimations are blurry and widespread over large areas) but it is recognized by its zero localization error in the absence of noise [16]. In its solution sLORETA introduces a non-linear standardization of the solution using the variance of the estimated activity $\boldsymbol{S}_x$, this variance is defined by:

$$\boldsymbol{S}_x = \boldsymbol{M}^T(\boldsymbol{M}\boldsymbol{M}^T + \lambda^2 I)^{-1}\boldsymbol{M} \tag{8}$$

The Eucledian distance was used to compute the localization error by comparing the position of the ground-truth source P_x and the estimated source position $P_{\hat{x}}$ using the follow equation:

$$LocE = \|P_x - P_{\hat{x}}\|_2 \tag{9}$$

Where $P_{\hat{x}}$ is selected from the estimated source activity $\hat{\boldsymbol{x}}$ by selecting the location of the source with the highest power value.

4 Results

A summary of the performed tests is presented in table 1. The localization error presented is the mean of the localization error across all epochs. We first evaluated the dataset with the three levels of added noise and constrained the search space to the 10-10 standard electrode placement. The localization error between the three levels of noise was similar, i.e. for 8 channels the errors were between 15.45 to 16.07 mm for sLORETA and 16.08 to 17.01 mm for wMNE. As the difference is less than 1 mm between the highest and lowest error for all electrode counts, we decided to continue the evaluations only with the dataset of higher noise level (0 dB).

The less accurate results were obtained when adding multiple constraints, in particular, the case when the optimization was performed in cascade with hemispherical symmetricity and search within the 10-10 system. The effect of these constraints increased the localization error between 2.01 and 3.34 mm in the lower channel counts of 8 and 16 channels when compared with only applying the 10-10 system constraint. On the contrary, when fewer constraints were imposed, the accuracy increased. As shown in the table 1, the highest accuracy values were obtained when no constraint was imposed or when only applying symmetricity constraint. These results coincide with the bigger search space of 339 channels, as no 10-10 system constraint was imposed in both cases. In these two cases, the localization error was lowered between 1.63 and 2.67 mm when compared with the 10-10 system constraint. The Pareto fronts when constraining the search space to 10-10 system and without constraint, search space of 339 channels, are presented in figure 2. It is noticeable that the Pareto fronts of sLORETA and wMNE were more accurate when not limiting the search space.

	Dataset	10dB	5dB	0dB				
	Constraint Type	10-10 system			10-10 system, Symmetricity, Cascade search	Symmetricity	No constraints	10-10 system, Cascade search
8 chs	sLORETA	15.87 (10.54)	15.45 (9.03)	16.07 (10.11)	18.59 (7.97)	**14.29 (5.04)**	14.74 (7.24)	16.75 (11.68)
	wMNE	16.08 (8.87)	16.19 (9.22)	17.01 (13.05)	19.49 (10.69)	14.94 (7.69)	**14.80 (10.84)**	16.64 (12.12)
16 chs	sLORETA	12.66 (9.10)	12.58 (9.04)	13.11 (8.77)	16.45 (9.58)	11.56 (5.57)	**10.69 (6.61)**	12.61 (9.09)
	wMNE	12.90 (8.92)	13.62 (8.82)	13.64 (8.89)	15.65 (8.87)	12.63 (5.11)	**12.01 (5.74)**	13.91 (9.19)
32 chs	sLORETA	7.80 (8.70)	7.85 (8.42)	7.74 (8.68)	8.42 (8.81)	6.02 (7.38)	**5.07 (5.64)**	8.41 (8.49)
	wMNE	7.30 (8.74)	7.32 (8.31)	6.45 (7.82)	7.20 (8.39)	**3.99 (6.37)**	5.18 (6.29)	6.62 (8.60)
72 chs	sLORETA	**4.00 (7.15)**	4.01 (7.15)	4.05 (7.16)	4.05 (7.16)	-	-	4.05 (7.16)
(10-10 system)	wMNE	3.77 (6.99)	3.75 (6.98)	**3.65 (6.99)**	**3.65 (6.99)**	-	-	**3.65 (6.99)**
339 chs	sLORETA	-	-	-	-	**0.00 (0.00)**	**0.00 (0.00)**	-
	wMNE	-	-	-	-	**0.00 (0.00)**	**0.00 (0.00)**	-

Table 1. Localization error (mm) and standard deviation of the optimization test. The values remarked correspond to the best result with a given number of channels and ESI method.

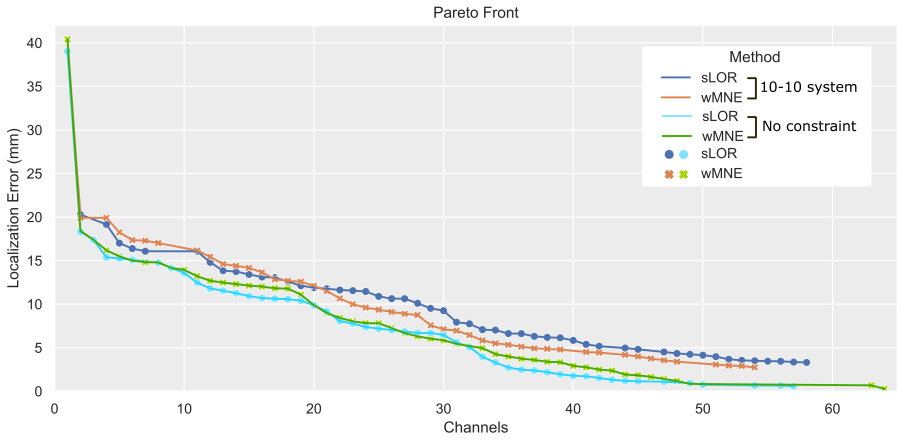

Fig. 2. Comparison of Pareto fronts for SNR 0 dB dataset when constraining the search space to the 10-10 positioning system and without constraining (search space of 339 positions).

The 8 channel combinations for the cases with the search space of 339 channels with and without symmetricity for sLORETA are presented in figure 3. From them, it can be seen that the electrodes were found close to the motor cortex areas, in both cases with one electrode slightly separate from the others.

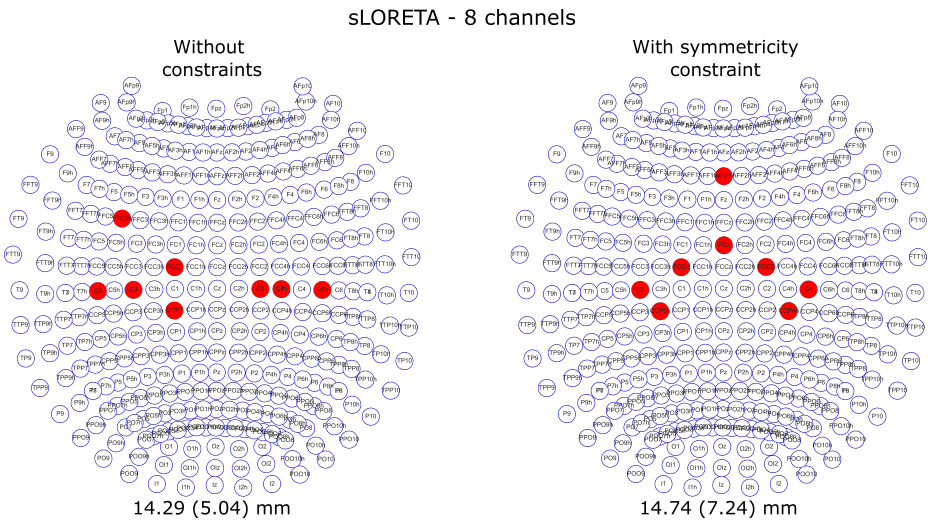

Fig. 3. Combinations of 8 channels for sLORETA without constraints and with symmetricity constraint.

5 Discussion and Conclusion

The localization error is an indication of the spatial accuracy, here, in the best evaluation cases we obtained 14.29 mm (8 channels, sLORETA, and only symmetricity constraint), 10.69 mm (16 channels, sLORETA, and no constraints), and 3.99 mm (32 channels, wMNE, and only symmetricity constraint). As in [22], we confirmed that the channel optimization with NSGA-II enables us to find channel combinations that led to the closest values to hdEEG accuracy values, in particular, the combination with 32 channels is less than 0.5 mm from the accuracy obtained with 72 channels in 10-10 system.

This research provides a pipeline to optimize the number of channels and identify ldEEG channel combinations for an individual subject that reduces the gap between hdEEG and ldEEG spatial accuracy. This systematic search for the best electrode positions was done as a first step in the design of dedicated EEG systems that can monitor the cortical source activity and facilitate the implementation of BCI systems for assisting in the rehabilitation of hand movement in stroke survivors. The previous studies in [3, 7, 12, 23] demonstrated that the source space can outperform the sensor space. Here, our results indicate that 16 channels could provide an accurate reconstruction to be used in BCIs related to hand movements.

The level of accuracy required for source-based BCIs for hand movements might depend on the type of imagined movements to classify. The boundaries of the applications should be clarified in further studies, i.e. it is noticeable that classifying between right or left hand might require lower spatial accuracy than classifying within wrist movements of the same limb.

The results indicate that when a bigger search space is used, better accuracy could be obtained. This should be considered in BCI systems, exploring electrode locations outside the standard positioning systems towards a personalized set of combinations can be valid in a BCI context if it leads to a better classification, future works should explore individual channel distributions and their classification performance. Here, we demonstrated that the use of electrode locations outside the standard led to lower reconstruction errors.

This work was limited to areas related to hand movements, the ROI was reduced to the hand knobs. Although the same procedure can be evaluated in other limbs or other regions of the brain. For example, to estimate the source activity of hearing-, visual-, or attention-related areas. To the best of our knowledge, no other studies have been conducted to evaluate the ESI properties on particular brain regions using ldEEG with optimized channel selection, and this framework can be generalized to particular ROIs. Here, the EEG simulation was limited to sinusoidal Gaussian activity and this may not fully capture the complex behavior of a real EEG recording. However, the simulation framework serves as basis to evaluate the spatial accuracy in the context of ldEEG source imaging, considering that the reduced spatial sampling has been one of the arguments against the use of source estimated activity in BCI systems. It is debatable whether increasing the complexity of the simulated signal will affect the spatial resolution, especially when considering that non-linear mix imposed by the volume conduction has been included during forward modeling.

In conclusion, this study explores the use of optimized ldEEG for estimating the source activity of the hand movement related areas and investigates the accuracy under multiple optimization scenarios. In this work, several key findings are reported. Firstly, optimized channel selection in ldEEG setups demonstrated potential as a viable alternative to hdEEG, offering a comparable accuracy when retrieving the source space of the particular ROI. This finding is significant as it paves the way for source-centered BCI systems with low EEG channel counts.

Moreover, we presented a comprehensive pipeline to perform channel optimization in the context of ESI. The pipeline can be used to identify the channels that can accurately estimate the sources in a ROI and to be used in developing customized EEG solutions for a particular user when using individual MRI for forward modeling.

Furthermore, as a result of the reduction of channels, the optimized ldEEG can improve the practicality of EEG in real-world scenarios, as fewer sensors often leads to wearable and easy-to-use devices. It can be argued that the estimation of the sources increases computational complexity, especially for online systems. However, pre-calculated forward models and inverse operators can serve to speed up the computations.

This work provides insights on the use of optimized ldEEG in retrieving sources towards BCI systems. However, several questions are still open and are required to be solved prior to implementation in BCI systems. Further studies should be performed to clarify the role of ESI with optimized sensors and to develop source-centered BCIs that can complement current BCI sytems based

on only scalp recordings. Also, to analyze the effect of optimized channels in the classification accuracy when using source and sensor space. Further efforts should be made to verify the implications of the source computation in online settings, and clarify whether to apply forward modeling on individual basis or to use brain structural information from template heads can be accurate enough.

References

1. Bradberry, T.J., Gentili, R.J., Contreras-Vidal, J.L.: Reconstructing three-dimensional hand movements from noninvasive electroencephalographic signals. Journal of Neuroscience **30**, 3432–3437 (3 2010). https://doi.org/10.1523/JNEUROSCI.6107-09.2010
2. Cincotti, F., Mattia, D., Aloise, F., Bufalari, S., Astolfi, L., Fallani, F.D.V., Tocci, A., Bianchi, L., Marciani, M.G., Gao, S., Millan, J., Babiloni, F.: High-resolution eeg techniques for brain–computer interface applications. Journal of Neuroscience Methods **167**, 31–42 (1 2008). https://doi.org/10.1016/J.JNEUMETH.2007.06.031
3. Edelman, B.J., Baxter, B., He, B.: Eeg source imaging enhances the decoding of complex right-hand motor imagery tasks. IEEE Transactions on Biomedical Engineering **63**, 4–14 (1 2016). https://doi.org/10.1109/TBME.2015.2467312
4. Fischl, B.: FreeSurfer. NeuroImage **62**(2), 774–781 (8 2012). https://doi.org/10.1016/J.NEUROIMAGE.2012.01.021
5. Fuchs, M., Wagner, M., Köhler, T., Wischmann, H.A.: Linear and nonlinear current density reconstructions (1999). https://doi.org/10.1097/00004691-199905000-00006
6. Fuchs, M., Wagner, M., Wischmann, H.A.: Generalized minimum norm least squares reconstruction algorithmss. ISBET Newsletter **5**(5), 8–11 (1994)
7. Giri, A., Kumar, L., Gandhi, T.: Cortical source domain based motor imagery and motor execution framework for enhanced brain computer interface applications. IEEE Sensors Letters **5** (12 2021). https://doi.org/10.1109/LSENS.2021.3122453
8. Gramfort, A., Luessi, M., Larson, E., Engemann, D.A., Strohmeier, D., Brodbeck, C., Goj, R., Jas, M., Brooks, T., Parkkonen, L., Hämäläinen, M.: Meg and eeg data analysis with mne-python. Frontiers in Neuroscience **0**, 267 (2013). https://doi.org/10.3389/FNINS.2013.00267/BIBTEX
9. Hardwick, R.M., Caspers, S., Eickhoff, S.B., Swinnen, S.P.: Neural correlates of action: Comparing meta-analyses of imagery, observation, and execution. Neuroscience & Biobehavioral Reviews **94**, 31–44 (11 2018). https://doi.org/10.1016/J.NEUBIOREV.2018.08.003
10. He, B., Baxter, B., Edelman, B.J., Cline, C.C., Ye, W.W.: Noninvasive brain-computer interfaces based on sensorimotor rhythms. Proceedings of the IEEE **103**, 907–925 (6 2015). https://doi.org/10.1109/JPROC.2015.2407272
11. He, B., Sohrabpour, A., Brown, E., Liu, Z.: Electrophysiological source imaging: A noninvasive window to brain dynamics. https://doi.org/10.1146/annurev-bioeng-062117-120853 **20**, 171–196 (6 2018). https://doi.org/10.1146/ANNUREV-BIOENG-062117-120853, https://www.annualreviews.org/doi/abs/10.1146/annurev-bioeng-062117-120853
12. Li, C., Guan, H., Huang, Z., Chen, W., Li, J., Zhang, S.: Improving movement-related cortical potential detection at the eeg source domain. International IEEE/EMBS Conference on Neural Engineering, NER pp. 214–217 (5 2021). https://doi.org/10.1109/NER49283.2021.9441169

13. Lotte, F., Bougrain, L., Cichocki, A., Clerc, M., Congedo, M., Rakotomamonjy, A., Yger, F.: A review of classification algorithms for eeg-based brain–computer interfaces: a 10 year update. Journal of Neural Engineering **15**, 031005 (4 2018). https://doi.org/10.1088/1741-2552/AAB2F2
14. Mattiocco, M., Babiloni, F., Mattia, D., Bufalari, S., Sergio, S., Salinari, S., Marciani, M.G., Cincotti, F.: Neuroelectrical source imaging of mu rhythm control for bci applications. Annual International Conference of the IEEE Engineering in Medicine and Biology - Proceedings pp. 980–983 (2006). https://doi.org/10.1109/IEMBS.2006.260128
15. Michel, C.M., Brunet, D.: Eeg source imaging: A practical review of the analysis steps. Frontiers in Neurology **10**, 325 (4 2019). https://doi.org/10.3389/fneur.2019.00325
16. Pascual-Marqui, R.D.: Standardized low-resolution brain electromagnetic tomography (sLORETA): technical details. Methods and findings in experimental and clinical pharmacology **24 Suppl D**, 5–12 (2002)
17. Pfurtscheller, G., Brunner, C., Schlögl, A., da Silva, F.H.L.: Mu rhythm (de)synchronization and eeg single-trial classification of different motor imagery tasks. NeuroImage **31**, 153–159 (5 2006). https://doi.org/10.1016/J.NEUROIMAGE.2005.12.003
18. Pfurtscheller, G., Silva, F.H.L.D.: Event-related eeg/meg synchronization and desynchronization: Basic principles. Clinical Neurophysiology **110**, 1842–1857 (11 1999). https://doi.org/10.1016/S1388-2457(99)00141-8
19. Saha, S., Baumert, M.: Intra- and inter-subject variability in eeg-based sensorimotor brain computer interface: A review. Frontiers in Computational Neuroscience **13**, 87 (1 2020). https://doi.org/10.3389/FNCOM.2019.00087/BIBTEX
20. Soler, A., Giraldo, E., Lundheim, L., Molinas, M.: Relevance-based Channel Selection for EEG Source Reconstruction: An Approach to Identify Low-density Channel Subsets. Proceedings of the 15th International Joint Conference on Biomedical Engineering Systems and Technologies, BIOSTEC **2, BIOIMAGING**, 174–183 (mar 2022). https://doi.org/10.5220/0010907100003123
21. Soler, A., Moctezuma, L.A., Giraldo, E., Molinas, M.: Automated methodology for optimal selection of minimum electrode subsets for accurate eeg source estimation based on genetic algorithm optimization. Scientific Reports 2022 12:1 **12**, 1–18 (7 2022). https://doi.org/10.1038/s41598-022-15252-0
22. Soler, A., Muñoz-Gutiérrez, P.A., Bueno-López, M., Giraldo, E., Molinas, M.: Low-Density EEG for Neural Activity Reconstruction Using Multivariate Empirical Mode Decomposition. Frontiers in Neuroscience **14**, 175 (feb 2020). https://doi.org/10.3389/fnins.2020.00175
23. Srisrisawang, N., Müller-Putz, G.R.: Applying dimensionality reduction techniques in source-space electroencephalography via template and magnetic resonance imaging-derived head models to continuously decode hand trajectories. Frontiers in Human Neuroscience **16**, 137 (3 2022). https://doi.org/10.3389/FNHUM.2022.830221/BIBTEX
24. Yuan, H., Doud, A., Gururajan, A., He, B.: Cortical imaging of event-related (de)synchronization during online control of brain-computer interface using minimum-norm estimates in frequency domain. IEEE Transactions on Neural Systems and Rehabilitation Engineering **16**, 425–431 (10 2008). https://doi.org/10.1109/TNSRE.2008.2003384